




Letter

Abrikosov clusters in chiral liquid crystal droplets

V Fernandez-Gonzalez^{1,*} , M G Clerc¹ , G González-Cortés¹ , P I Hidalgo² 
and J Vergara² 

¹ Departamento de Física and Millennium Institute for Research in Optics, Facultad de Ciencias Físicas y Matemáticas, Universidad de Chile, Casilla 487-3, Santiago, Chile

² Departamento de Química Orgánica, Facultad de Ciencias Químicas, Universidad de Concepción, Casilla 160-C, Concepción, Chile

E-mail: victor.fernandez.g@ug.uchile.cl

Received 11 August 2024, revised 25 October 2024

Accepted for publication 14 November 2024

Published 21 November 2024

Corresponding editor: Dr Lorna Brigham



Abstract

Self-organizing triangular lattices of topological vortices have been observed in type-II superconductors, Bose–Einstein condensates, and chiral magnets under external forcing. Liquid crystals exhibit vortex self-organization in dissipative media. In this study, we experimentally investigate the formation of vortex clusters, analogous to Abrikosov lattices, in temperature-driven chiral liquid crystal droplets. Based on a Ginzburg–Landau-like equation, we derive the interaction laws underlying the formation of these Abrikosov clusters of chiral domains. The origin of these is elucidated due to the competition between the repulsive interaction and the spatial effect of the confinement within the droplet. Our results advance the theoretical understanding of localized vortex self-organization in liquid crystals and open up possibilities for controlling the clustering of these topological defects.

Supplementary material for this article is available [online](#)

Keywords: liquid crystals, chirality, confinement, clustering, Ginzburg–Landau equation, topological defects, vortices

Certain conductive materials become superconductors at very low temperatures [1, 2]; that is, the electric current through the material does not present resistance. Furthermore, the Meissner effect causes the superconductor to levitate in the presence of a magnetic field, which cannot penetrate the superconductor. As the magnetic field strength or temperature increases, the magnetic field in type-II superconductors begins to penetrate the material at certain points. These penetration points correspond to vortices in the amplitude of the

superconducting wave function described by the Ginzburg–Landau equation, as established by Abrikosov [3]. Due to the repulsion between the vortices and the confinement of the applied magnetic field, the vortices self-organize into a triangular lattice [3]. This type of vortex arrangement is commonly referred to as an Abrikosov lattice. This phenomenon has been observed in superconductors [4, 5] and Bose–Einstein condensates [6] under external forcing. Similarly, thermally controlled magnetic materials forced by a magnetic field exhibit triangular lattices of skyrmions, called the A-phase in chiral magnets [7, 8]. Triangular lattices of localized vortices or chiral domains have also been observed in dissipative systems

* Author to whom any correspondence should be addressed.

such as chiral liquid crystal cells [9–12]. These topological defects, also known as chiral bubbles or domains, are generated as the folding of chiral fingers observed in labyrinthine cholesteric patterns or in the isotropic-chiral nematic phase transition [12, 13]. Figure 1(a) illustrates the typical triangular lattice observed from the transition between isotropic to chiral nematic phase in a liquid crystal layer. Since the medium is chiral, only chiral domains with a positive topological charge are stable. This charge accounts for the direction of the director vector around the vortex position, which rotates clockwise around it. Vortices of the same charge repel each other [14]. References [15, 16] present a detailed study of the three-dimensional structure of these chiral domains employing confocal microscopy, numerical simulations, group theory, and algebraic geometry, where they are described as elementary liquid crystal torons. Typically, chiral domains are created from labyrinthine patterns that generate a spatially random distribution of chiral bubbles (cf figure 1(b)). Because of the weak interaction, no self-interaction of the chiral bubbles is observed. The interaction between chiral domains has been qualitatively characterized [17], and free energy terms have been identified [18]. In addition, based on an appropriate ansatz for chiral domains of the free energy in three dimensions, an exponential and inverse square root of distance interaction law was established and experimentally observed [19].

This letter aims to study the self-organization of localized vortices in confined geometries, liquid crystal droplets (see figure 1). Experimentally, we study the formation of clusters of chiral domains based on temperature-driven chiral nematic liquid crystal droplets. We have coined these arrangements as *Abrikosov clusters*. Employing a chiral-anisotropic Ginzburg–Landau equation with inhomogeneous parameters, valid near the winding/unwinding transition, we numerically observe the formation of Abrikosov clusters of chiral domains. The repulsive interaction between vortices, as well as the effect of the inhomogeneity induced by the droplet, are analytically characterized. The competition between the repulsive interaction of chiral bubbles and spatial confinement has been identified as the origin of these clusters. The results of the numerical simulations are in good qualitative agreement with the experimental findings.

1. Experimental setup

The temperature-driven chiral liquid crystal droplet setup is illustrated in figure 1(c). A polarized optical microscope (POM, Leica DM2700P) was used to examine the droplets placed on a glass slide inside a thermal control microscope stage (TC, Mod. LTS350E c/4 Elect LINKAM). The temperature and heat rate in the liquid crystal can be controlled and monitored at this stage with a precision of $0.01 \pm 0.005 \text{ } ^\circ\text{C min}^{-1}$. Light from a white LED source (WLS) is transmitted through a polarizer P to illuminate the liquid crystal droplets. The objective O captures the transmitted light, reaching an analyzer A cross-polarized to the polarizer P . A complementary metal-oxide-semiconductor (CMOS, Thorlabs CS126CU) camera captures the transmitted light.

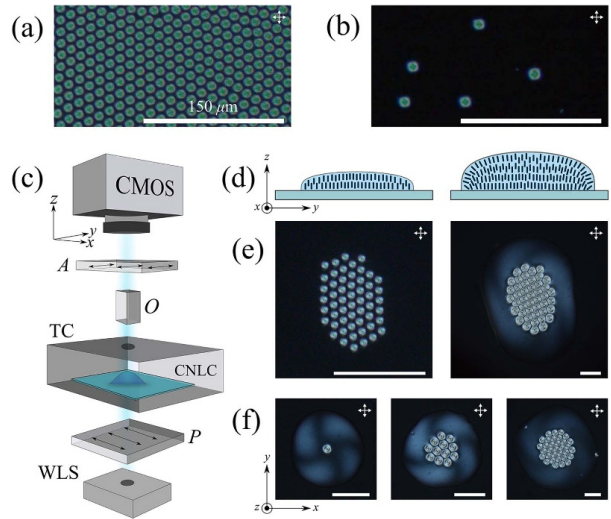


Figure 1. Experimental observation of Abrikosov clusters in chiral liquid crystal droplets. Triangular lattice (a) and spatial random distribution (b) of vortices observed in a chiral liquid crystal cell with homeotropic anchoring. (c) Schematic representation of the experimental setup. A chiral nematic liquid crystal (CNLC) droplet is placed over a glass slide inside a thermal chamber (TC) and illuminated by a white LED light source (WLS). The analyzer, objective, and polarizer are represented by A , O , and P , respectively. The two polarizers A and P are orthogonal, *cross-polarization*. The CNLC is monitored by a complementary metal–oxide–semiconductor (CMOS) camera. (d) Schematic representation of the average molecular alignment for different concentrations of the chiral molecule EOS-12 at 10 and 3 wt%. A homeotropic state and orthogonal anchoring to the surface characterize small and large droplet. (e) Abrikosov cluster on a droplet for different concentrations of chiral molecules at 10 (left panel) and 3 (right panel) wt%. (f) Formation of clusters with different numbers of clustered vortices at a concentration of 3 wt%. The white double arrows represent the crossed polarization. Scale bars are $150 \mu\text{m}$ in all images.

The droplets were generated by capillary deposition using a $0.2\text{--}2 \mu\text{l}$ micropipette over a soda-lime glass slide (EDLAB Cat. No. 7105). Note that we have no control over the exact shape of the droplet and its contact angle (see figure 1). The untreated glass slide displayed a homeotropic alignment for the liquid crystal droplet (see figure 1(d) for a schematic representation of the average molecular alignment within the droplet). The chiral nematic liquid crystal utilized in this experiment comprises E7 (Merck) as the nematic host and EOS-12 as the chiral molecule (for details on this molecule see [20]). Mesophase characterization as a function of temperature and concentration of the liquid crystal mixture is available in [21].

2. Experimental Abrikosov cluster

Initially, the droplet is heated to a temperature of $80 \text{ } ^\circ\text{C}$, which is above the chiral nematic-isotropic phase transition. After reaching the set temperature, the system is cooled down to $18 \text{ } ^\circ\text{C}$ (room temperature) in approximately 10 min.

The droplet transitions from an isotropic liquid phase to a chiral liquid crystal one, and as the liquid crystal winds in the chiral phase, localized vortices are nucleated inside the droplet [22], and they self-organize into a clustered triangular lattice, *Abrikosov cluster*. To study the dynamics of chiral domains in thermal equilibrium, the system is monitored after one hour at room temperature. Figures 1(e) and (f) show typical Abrikosov clusters observed in the liquid crystal droplets with different concentrations of chiral molecules. This triangular cluster is a consequence of two facts: (i) the system maximizes the chiral energy by creating chiral domains (bubbles) that repel each other, and (ii) the inhomogeneity of the droplet induces the chiral domains to migrate toward the center of it (cf figure 1(e)). The formation of Abrikosov clusters is observed for droplets of different sizes. Note that as the concentration of the chiral molecules decreases, the size of the chiral domains increases [23]. To facilitate the observation of the formation of the Abrikosov cluster in large droplets, we considered a lower concentration of the chiral molecules (cf figure 1(e)). In the case of small droplets (with a diameter of about 200 μm), we observe that the background of the chiral domains is in a homeotropic state, i.e. the background is dark. On the contrary, a structure of four brushes is observed as a background for large droplets (diameter larger than 200 μm). This indicates that the molecules are anchored perpendicular to the surface of the droplet [24]. Figure 1(d) illustrates the anchoring of small and large droplets. Likewise, we observe different triangular clusters for droplets with the same concentration of chiral molecules but different sizes, as illustrated in figure 1(f).

3. Theoretical description

Chiral nematic liquid crystals are characterized by the fact that the molecules locally have an orientation order but not a positional one [12, 24]. This average molecular orientation is characterized by a director vector $n(\vec{r}, t)$, where \vec{r} and t represent the spatial coordinate and time. Likewise, on a macroscopic level, chirality manifests itself by generating a rotation of the director vector, which accounts for a collective rotation of many molecules. The rotation step is called pitch [12, 24] and is represented by the parameter p . For a chiral liquid crystal thin film with homeotropic anchoring, the director is described by

$$\mathbf{n} = \begin{pmatrix} \cos\left(\frac{z}{p} + \theta\right) \sin\left[\alpha \sin\left(\frac{\pi z}{d}\right)\right] \\ \sin\left(\frac{z}{p} + \theta\right) \sin\left[\alpha \sin\left(\frac{\pi z}{d}\right)\right] \\ \cos\left[\alpha \sin\left(\frac{\pi z}{d}\right)\right] \end{pmatrix}, \quad (1)$$

where $\alpha(x, y, t)$ and $\theta(x, y, t)$ account for the polar and azimuthal angles the director forms concerning the vertical direction. z represents the vertical coordinate of the thin film thickness. d denotes the thickness of the thin liquid crystal film. The minimization of the Frank–Oseen free energy characterizes the dynamics of the director [12, 24].

Due to elastic coupling, homeotropic anchoring, and confinement effects on the chiral liquid crystals, the system minimizes the free energy through a completely vertical configuration in a homeotropic state as the temperature decreases. Namely, the homeotropic state is described by $\alpha=0$ and $\mathbf{n}=(0,0,1)$. This state is often referred to as the unwound state. Experimentally, it is characterized by the droplet becoming completely dark under crossed polarizers. As the temperature increases, the homeotropic state becomes unstable, characterized by the manifestation of a chiral state, chiral domains, and cholesteric fingers [12, 24]. This transition is known as a winding/unwinding transition and is of the first order type, i.e. it is characterized by exhibiting hysteresis [22]. Taking into account that the director is slightly deformed from the z -axis ($\alpha \ll 1$), the order parameter that characterizes this transition is $Q(x, y, z, t) \equiv n_z(n_x + in_y) \approx Ae^{iz/p} \sin(\pi z/d)$ [25], where the two-dimensional complex amplitude $A(x, y, t) \equiv \alpha(x, y, t)e^{i\theta(x, y, t)}$ accounts for the projection of the director into the xy -plane. Considering the equation of the director close to the winding/unwinding transition, using expression (1) for small α , and through weakly nonlinear analysis, amplitude A satisfies the equation (dimensionless chiral-anisotropic Ginzburg–Landau amplitude equation) [13, 22]

$$\partial_t A = \mu A + \beta A|A|^2 - A|A|^4 + \partial_{\eta\bar{\eta}} A + \delta \partial_{\eta\bar{\eta}} \bar{A} + \chi (A \partial_{\bar{\eta}} A - \bar{A} \partial_{\eta} A), \quad (2)$$

where

$$\begin{aligned} \mu &= \frac{\pi^2}{d^2} \left(2C - \frac{K_3}{K_2} \right), \\ \beta &= -\frac{\pi^2}{d^2} \left(3 + \frac{K_1}{K_2} - 6\frac{K_3}{K_2} + 6C \right), \\ \delta &= \frac{K_1 - K_2}{K_1 + K_2}, \\ \chi &= \left(\frac{16}{5Q} \right)^{1/4} \frac{3 - 4\frac{K_3}{K_2} + \frac{K_1}{K_2} + 3C}{2\sqrt{2}\sqrt{1 + \frac{K_1}{K_2}}}, \end{aligned} \quad (3)$$

K_1 , K_2 , and K_3 account for the splay, twist, and bend elastic constants, $C \equiv d/p$ stands for the confinement parameter, and $Q \equiv K_3/K_2 - 0.53K_1/K_2 - 2.1K_3/K_2 + 0.22K_1/K_3 + 1.18$. $\partial_{\eta} \equiv \partial_x + i\partial_y$ is the differential operator on the complex plane, the Wirtinger derivative. \bar{A} accounts for the complex conjugate A . The pitch p is a decreasing function of the concentration of the chiral dopants and the temperature [21]. The explicit expression for pitch as a function of chiral molecule concentration and temperature is unknown; however, an experimental fit shows that the pitch decays inversely with concentration [21]. Thus, the chirality parameter χ grows linearly with the concentration of chiral molecules. Note that μ is the control parameter, which is proportional to the temperature minus the critical temperature of the transition, and β , δ , and χ account for the nonlinear response, anisotropic, and chiral coupling, respectively. In [13], a detailed derivation of the amplitude equation (2) is reported.

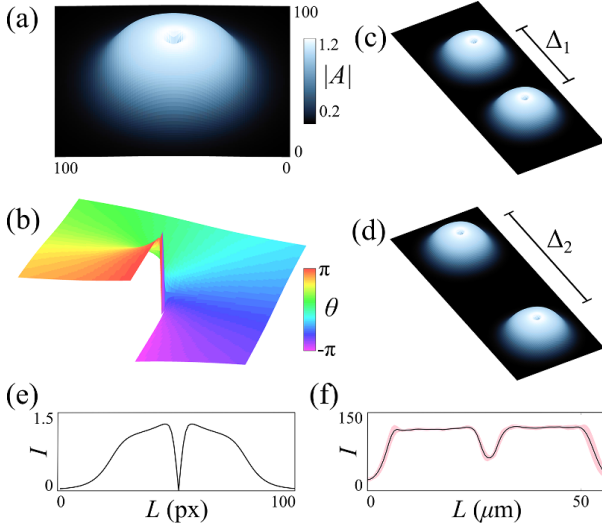


Figure 2. Chiral domains and interaction between them of the dimensionless chiral-anisotropic Ginzburg–Landau amplitude equation (2) with $\mu = -0.2$, $\beta = 1$, $\delta = 0.25$, and $\chi = 0.7$. (a) Magnitude $|A|$ and (b) phase θ of the amplitude $A = |A|e^{i\theta}$ of a chiral domain. The phase jump indicates the presence of a topological defect. (c), (d) Schematic representation of the repulsive interaction between vortices, where Δ accounts for the distance between vortices, $\Delta_1(t_1) < \Delta_2(t_2)$, with $t_1 < t_2$. (e), (f) Numerical profile and experimental transverse light intensity profile of chiral domains. The red area around the experimental profile represents the measured standard deviation of eight different vortices along their brightest section.

4. Numerical Abrikosov cluster

The amplitude equation (2) is variational and has been used to understand chiral domains, cholesteric fingers, disordered patterns, and topological transitions in chiral liquid crystals [12, 13, 22, 26]. For this purpose, we proceed by integrating the amplitude equation (2) on a square grid with periodic boundary conditions, using a spectral method and a fourth-order Runge–Kutta scheme (see supplemental material for more details). Figures 2(a) and (b) show the amplitude magnitude $|A|$ and phase θ of a chiral domain. Note that only stable chiral domains with positive topological charges are observed. Likewise, when two chiral domains are considered, they repel each other with a weak force, as illustrated in figures 2(c) and (d). Figures 2(e) and (f) show the profile of the numerical and experimental chiral domains.

The parameters of the amplitude equation depend on the thickness of the liquid crystal sample (cf set of formulas 3). Hence, the parameters are expected to become inhomogeneous to model the droplet effect. The small control parameter μ is most affected because the other parameters are of order one (cf supplemental material). Therefore, we promote this parameter as a function of the spatial coordinates. Due to the symmetry of the droplets, we consider

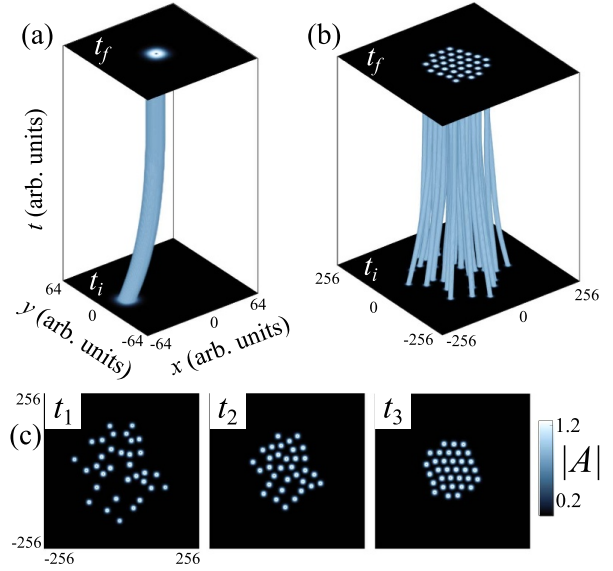


Figure 3. Numerical Abrikosov cluster of the dimensionless chiral-anisotropic Ginzburg–Landau amplitude equation (2) with an inhomogeneous bifurcation parameter $\mu(r) = \mu_0 + \mu_1 r^2$, $\beta = 1$, $\delta = 0.25$, and $\chi = 2.4$. (a), (b) spatiotemporal counterplot of single and multiple chiral domains interacting with $\mu_0 = -0.55$ and $\mu_1 = -2 \times 10^{-5}$, respectively. The colormaps consider the initial and final states t_i and t_f . (c) Time series of snapshots considering the clustering of multiple vortices into an Abrikosov cluster, where $t_1 < t_2 < t_3$.

for simplicity a parabolic shape $\mu(r) = \mu_0 + \mu_1 r^2$, where r represents the polar radial coordinates with the origin at the position of the maximum height of the droplet (center of the droplet). Assuming that the droplet thickness is deformed as $d = d_0 + d_1 r^2$, then $\mu_0 \equiv \pi^2(2d_0/p - K_3/K_2)/d_0^2$ and $\mu_1 = 2\pi^2 d_1/d_0^2 p - 2\pi^2 d_1(2d_0/p - K_3/K_2)/d_0^3 p$. Figure 3 shows numerical simulations of the amplitude equation (2) with inhomogeneous bifurcation parameters $\mu(r)$, showing chiral domains propagating towards the origin of the coordinate system $\mu(r=0)$. Note that if one considers other even polynomials for $\mu(r)$, one observes the same formation of vortex clusters qualitatively. Figures 3(a) and (b) show the spatiotemporal evolution of the amplitude A for single and multiple chiral domains. Furthermore, figure 3(c) shows a colormap time sequence of the spatiotemporal diagram illustrated in figure 3(b). From these charts, we conclude that the localized vortices self-organize into a triangular cluster as an effect of the repulsive interaction between them and the confinement effect induced by the inhomogeneous bifurcation parameter.

To figure out the origin of the self-organization that gives rise to the Abrikosov cluster, we must characterize both the repulsive interaction between chiral bubbles and the influence of the inhomogeneity given by the spatial constraint of the droplet to induce the clustering of the chiral domains. Therefore, to determine the interaction, we consider two chiral

domain solutions whose positions are initially at a distance Δ_0 from each other. Let us consider the following ansatz for the chiral domain pair

$$A(\mathbf{r}, t) \equiv R_1(\mathbf{r} + \Delta(t)\hat{r}/2)e^{i\phi_1(\mathbf{r}, \Delta(t))} + R_2(\mathbf{r} - \Delta(t)\hat{r}/2)e^{i\phi_2(\mathbf{r}, \Delta(t))} + W(\mathbf{r}, \Delta(t)), \quad (4)$$

where the coordinate system is positioned at the midpoint between both chiral domains. $\{R_1, \phi_1\}$ and $\{R_2, \phi_2\}$ are the magnitude and phase of the respective chiral domains positioned in $-\Delta/2\hat{r}$ and $\Delta/2\hat{r}$, respectively. $\Delta(t)$ is the distance between chiral domains. $W(\mathbf{r}, \Delta(t))$ accounts for a small correction that becomes smaller as Δ increases. Replacing the ansatz (4) in equation (2), considering that the chiral domains are sufficiently separated, linearizing in W , and imposing a solvability condition, after straightforward calculations, one obtains at dominant order

$$\begin{aligned} \dot{\Delta} \approx & -\frac{2\beta}{3} \frac{\int_0^\infty \partial_z R_1^3 \frac{e^{-2\epsilon(z+\Delta)}}{\sqrt{z+\Delta}} dz}{\int_0^\infty (\partial_z R_1)^2 dz} \\ & - \frac{\epsilon\chi \int_0^\infty \partial_z R_1 \frac{e^{-2\epsilon(z+\Delta)}}{\sqrt{z+\Delta}} dz}{\int_0^\infty (\partial_z R_1)^2 dz} \approx \mathcal{I} \frac{e^{-2\epsilon\Delta}}{\sqrt{\Delta}}, \end{aligned} \quad (5)$$

where $\epsilon = \sqrt{|\mu|/(1+\delta)}$ characterizes the spatial decay of chiral domains and \mathcal{I} is a positive constant. Consequently, the chiral domains exhibit an exponential kinematic repulsion law, resulting in a logarithmic growth of the distance over time. This phenomenon is characterized by the slow movement of the chiral domains away from each other. The interaction between chiral domains has been calculated, motivated by the skyrmion bags observed in liquid crystals and ferromagnets [19]. Based on the ansatz for chiral domains in liquid crystals and free energy in three dimensions, the same interaction law, formula (5), has been found and observed experimentally. In the case of ferromagnets, the formula (5) does not adequately describe the results, which can be improved by including magnetic dipolar moment interaction effects. Note that a similar interaction law is obtained for localized precession states on a flat ferromagnetic layer subjected to a magnetic field [27].

As we have mentioned, to model the spatial confinement caused by the droplet, one can consider a single chiral domain subjected to a weakly spatial inhomogeneity $\mu(r) = \mu_0 + \mu_1 r^2$ with $\mu_1 \ll 1$. Introducing the ansatz $A = A_v(\vec{r} - \vec{x}_0(t)) + \mathcal{W}(\vec{x}_0(t), \vec{r})$, where $A_v = R(r)e^{i\theta}$ is the vortex solution of the homogeneous equation (2), $\vec{x}_0 = (x_0, y_0)$ is the vector that account for the vortex position with respect to the droplet center, assuming that $\vec{x}_0(t)$ slow varying temporal vector ($\partial_t \vec{x}_0 \ll 1$), and \mathcal{W} small correction function. Introducing the previous ansatz in equation (2), linearizing in \mathcal{W} and after straightforward calculations, we get

$$\partial_t \vec{x}_0 = -\mathcal{J}^2 \vec{x}_0, \quad (6)$$

where $\mathcal{J}^2 = -\int_0^\infty r^2 \partial_r R^2 dr / \int_0^\infty 2r[(\partial_r R)^2 + R^2/r] dr$. Then, the vortex tends to move toward the center of the droplet.

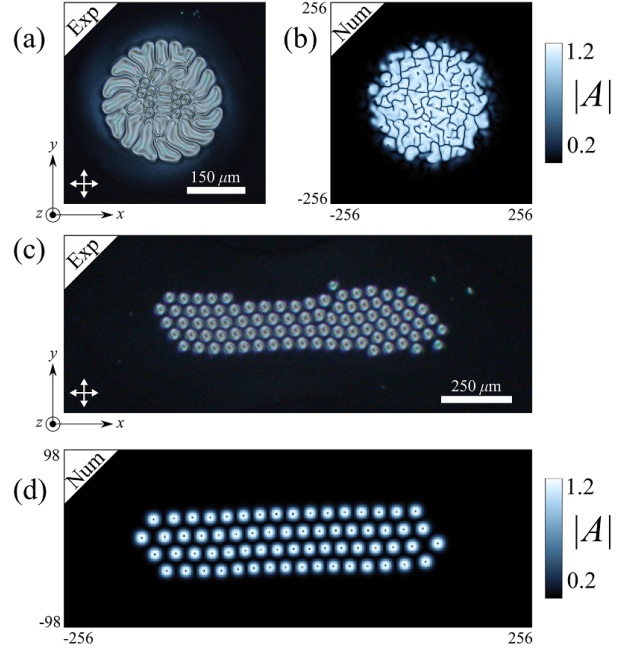


Figure 4. Transition states and irregular droplets in chiral nematic liquid crystal droplets. (a), (b) Experimental and numerical transition states from chiral to isotropic state formed inside the droplets, respectively. Both states represent the evolution of chiral domains from chiral textures. (c) Abrikosov cluster formed in an irregular elongated droplet for 10 wt% of the chiral mixture. (d) Chiral domains self-organization over an irregular potential $\mu(r) = ax^2 + by^2 + c$, where $a = -2 \times 10^{-5}$, $b = -2 \times 10^{-7}$, and $c = -0.55$. The other parameters used for the numerical simulations were $\beta = 1$, $\delta = 0.25$, and $\chi = 2.4$. The white double arrows represent the crossed polarization.

Namely, the set of equations (6) indicates that the vortex moves against the slope imposed by the inhomogeneity. Therefore, it is expected that by incorporating an inhomogeneous potential in equation (2), a chiral bubble should move to the maximum value of μ as long as it is in the range of existence of chiral domains [22]. Note that in the previous analysis we considered a slight variation in the thickness of the droplet to perform our analytical study. In the case of confinement with more realistic shapes, the analytical calculations are valid only near the central region; towards the droplet boundary, the chiral domains are strongly deformed, which does not allow perturbative calculations, and only numerical simulations allow us to perform the analysis.

In the case of multiple solutions, since the interaction described by equation (5) is repulsive and the inhomogeneous parameter induces the clustering (see set of equation (6)), the chiral domains self-organize into an Abrikosov cluster. Hence, this inhomogeneity allows us to study the effect of the confinement imposed by the droplet, it is also possible to study other types of observed textures, such as transition states that appear in the vicinity of the chiral nematic-isotropic phase transition and different droplet shapes, which allow to control the self-organization of the vortices.

Figure 4 shows the correspondence between numerical results and experimental observations for both the transition state and the case of a droplet with a non-axisymmetric shape. In the latter case, we consider a bifurcation parameter $\mu(x, y)$ with an elongated shape in one direction (cf figure 4).

In conclusion, based on an amplitude equation close to the unwinding/winding transition and temperature-driven chiral liquid crystal droplets, we have demonstrated theoretically and experimentally the self-organization mechanisms of chiral domains that give rise to Abrikosov clusters in dissipative media. The observed phenomenon is the dissipative counterpart of the triangular lattice or Abrikosov lattice, observed in conservative systems such as driven superconductors, Bose–Einstein condensates, and chiral magnetic systems.

Numerically, we could reproduce the experimental observations of temperature-driven CNLC droplets in fair qualitative agreement. A similar triangular vortex lattice is generated for curved smectic liquid crystals (see review [28] and references therein), as well as other forms of droplet-like confinement such as a Janus shell [29]. An amplitude equation approach, such as equation (2), may allow an understanding of the emergence of this type of self-organization. Note that as light passes through a droplet configuration, it acquires chirality via the chiral domains [30]. Optical vortex clusters are essential for developing data transmission [31] and improving astronomical imaging [32], because they contain multiple optical vortices that provide information, flexibility, and manipulation. Our results open the way for future studies on the control and applications of topological defects in chiral materials and provide a theoretical framework for studying systems with similar defects, such as chiral magnets and chiral ferromagnetic liquid crystal colloids [33]. Although the equilibria one expects to observe should be similar, the dynamics of chiral domains in conservative and dissipative systems differ significantly.

As mentioned, chiral domains are nucleated by heating the system above the chiral nematic-isotropic transition temperature and then cooling it to room temperature. In this initial process, the chiral domains begin to rearrange and interact out of thermal equilibrium. Thermal gradients can induce molecular reorientation, *thermophoresis* [34–37]. This physical process may be critical to understanding these initial transients and the creation of clusters of chiral domains. Work in this direction is ongoing. Moreover, it has been shown that chiral domains driven by oscillating fields exhibit propagation [38, 39]. Our approach based on amplitude equations can help to understand the dynamics of these propagative chiral domains.

Data availability statement

The data that support the findings of this study are available upon reasonable request from the authors.

Acknowledgments

The authors thank S Echeverría-Alar for fruitful discussions. V F-G, M G C, and G G-C acknowledge the financial support of ANID-Millennium Science Initiative Program-ICN17_012 (MIRO) and FONDECYT, Chile Project No. 1210353.

ORCID iDs

V Fernandez-Gonzalez  <https://orcid.org/0000-0002-6652-6131>

M G Clerc  <https://orcid.org/0000-0002-8006-0729>

G González-Cortés  <https://orcid.org/0000-0003-3548-2380>

P I Hidalgo  <https://orcid.org/0000-0002-6668-9950>

J Vergara  <https://orcid.org/0000-0001-7417-4925>

References

- [1] De Gennes P-G 2018 *Superconductivity of Metals and Alloys* (CRC Press)
- [2] Tinkham M 2004 *Introduction to Superconductivity* (Courier Corporation)
- [3] Abrikosov A A 1957 The magnetic properties of superconducting alloys *J. Phys. Chem. Solids* **2** 199
- [4] Essmann U and Träuble H 1967 The direct observation of individual flux lines in type II superconductors *Phys. Lett. A* **24** 526
- [5] Hess H, Robinson R, Dynes R, Valles J Jr and Waszczak J 1989 Scanning-tunneling-microscope observation of the Abrikosov flux lattice and the density of states near and inside a fluxoid *Phys. Rev. Lett.* **62** 214
- [6] Abo-Shaeer J R, Raman C, Vogels J M and Ketterle W 2001 Observation of vortex lattices in Bose–Einstein condensates *Science* **292** 476
- [7] Mühlbauer S, Binz B, Jonietz F, Pfleiderer C, Rosch A, Neubauer A, Georgii R and Böni P 2009 Skyrmion lattice in a chiral magnet *Science* **323** 915
- [8] Yu X Z, Onose Y, Kanazawa N, Park J H, Han J H, Matsui Y, Nagaosa N and Tokura Y 2010 Real-space observation of a two-dimensional skyrmion crystal *Nature* **465** 901
- [9] Kawachi M, Kogure O and Kato Y 1974 Bubble domain texture of a liquid crystal *Jpn. J. Appl. Phys.* **13** 1457
- [10] Haas W E and Adams J E 1974 Electrically variable diffraction in spherulitic liquid crystals *Appl. Phys. Lett.* **25** 263
- [11] Bhide V, Jain S and Chandra S 1977 Structure and properties of bubble domains in cholesteric-nematic mixtures *J. Appl. Phys.* **48** 3349
- [12] Oswald P and Pieranski P 2005 *Nematic and Cholesteric Liquid Crystals* (CRC Press)
- [13] Echeverría-Alar S, Clerc M G and Bordeu I 2023 Emergence of disordered branching patterns in confined chiral nematic liquid crystals *Proc. Natl Acad. Sci. USA* **120** e2221000120
- [14] Pismen L M 1999 *Vortices in Nonlinear Fields: From Liquid Crystals to Superfluids, From Non-Equilibrium Patterns to Cosmic Strings* vol 100 (Oxford University Press)
- [15] Smalyukh I I, Lansac Y, Clark N A and Trivedi R P 2010 Three-dimensional structure and multistable optical switching of triple-twisted particle-like excitations in anisotropic fluids *Nat. Mater.* **9** 139

- [16] Wu J S and Smalyukh I I 2022 Hopfions, heliknotons, skyrmions, torons and both abelian and nonabelian vortices in chiral liquid crystals *Liq. Cryst. Rev.* **10** 34–68
- [17] Ackerman P J, Qi Z and Smalyukh I I 2012 Optical generation of crystalline, quasicrystalline and arbitrary arrays of torons in confined cholesteric liquid crystals for patterning of optical vortices in laser beams *Phys. Rev. E* **86** 021703
- [18] Leonov A O, Draganov I E, Röbber U K and Bogdanov A N 2014 Theory of skyrmion states in liquid crystals *Phys. Rev. E* **90** 042502
- [19] Foster D, Kind C, Ackerman P J, Tai J S B, Dennis M R and Smalyukh I I 2019 Two-dimensional skyrmion bags in liquid crystals and ferromagnets *Nat. Phys.* **15** 655
- [20] Parra M L, Hidalgo P I and Elgueta E Y 2008 Synthesis and mesomorphic properties of oxadiazole esters derived from (*R*)-2-octanol, (*S*)-2-*n*-octyloxypropanol and (2*S*, 3*S*)-2-chloro-3-methylpentanol *Liq. Cryst.* **35** 823
- [21] Clerc M G, Cornejo A H, Echeverría-Alar S, González-Cortés G, Hidalgo P I, Luo P J, Morel M J, Vergara J and Wilson M 2023 Chirality transfer to harness mesophase transitions in liquid crystal mixtures containing an oxadiazole derivative *Liq. Cryst.* **50** 1938
- [22] Clerc M G, González-Cortés G and Echeverría-Alar S 2022 Localized dissipative vortices in chiral nematic liquid crystal cells *Phys. Rev. Res.* **4** L022021
- [23] Kerllenevich B and Coche A 1981 Bubble domain in cholesteric liquid crystals *Mol. Cryst. Liq. Cryst.* **68** 47
- [24] de Gennes P and Prost J 1993 *The Physics of Liquid Crystals* (*International Series of Monographs on Physics*) (Clarendon)
- [25] Frisch T, Gil L and Gilli J M 1993 Two-dimensional Landau-De Gennes dynamical model for the unwinding transition of a cholesteric liquid crystal *Phys. Rev. E* **48** R4199
- [26] Fernandez-Gonzalez V, Echeverría-Alar S, Vergara J, Hidalgo P I and Clerc M G 2024 Topological transition between disordered patterns through heating rate-induced defect emergence *Chaos Solitons Fractals* **180** 114508
- [27] Clerc M G, Coulibaly S and Laroze D 2010 Interaction law of 2D localized precession states *Europhys. Lett.* **90** 38005
- [28] Kim D S and Yoon D K 2018 Curvatures of smectic liquid crystals and their applications *J. Inf. Disp.* **19** 7
- [29] Durey G, Sohn H R O, Ackerman P J, Brasselet E, Smalyukh I I and Lopez-Leon T 2020 Topological solitons, cholesteric fingers and singular defect lines in Janus liquid crystal shells *Soft Matter* **16** 2669–82
- [30] Marrucci L, Manzo C and Paparo D 2006 Optical spin-to-orbital angular momentum conversion in inhomogeneous anisotropic media *Phys. Rev. Lett.* **96** 163905
- [31] Wang J *et al* 2012 Terabit free-space data transmission employing orbital angular momentum multiplexing *Nat. Photon.* **6** 488
- [32] Aleksanyan A and Brasselet E 2016 Vortex coronagraphy from self-engineered liquid crystal spin-orbit masks *Opt. Lett.* **41** 5234
- [33] Zhang Q, Ackerman P J, Liu Q and Smalyukh I I 2015 Ferromagnetic switching of knotted vector fields in liquid crystal colloids *Phys. Rev. Lett.* **115** 097802
- [34] Currie P K 1973 The orientation of liquid crystals by temperature gradients *Rheol. Acta* **12** 165
- [35] Di Leonardo R, Ianni F and Ruocco G 2009 Colloidal attraction induced by a temperature gradient *Langmuir* **25** 4247
- [36] Kim Y K, Senyuk B and Lavrentovich O D 2012 Molecular reorientation of a nematic liquid crystal by thermal expansion *Nat. Commun.* **3** 1133
- [37] Sarman S and Laaksonen A 2014 Director alignment relative to the temperature gradient in nematic liquid crystals studied by molecular dynamics simulation *Phys. Chem. Chem. Phys.* **16** 14741
- [38] Sohn H R O, Liu C D and Smalyukh I I 2019 Schools of skyrmions with electrically tunable elastic interactions *Nat. Commun.* **10** 4744
- [39] Sohn H R O and Smalyukh I I 2020 Electrically powered motions of toron crystallites in chiral liquid crystals *Proc. Natl Acad. Sci. USA* **117** 6437